Suplemento de la Revista Mexicana de Física **3** 010606 (2022) 1–6

Transport and concentration of uranium isotopes in the Laguna del Cuervo, Chihuahua, Mexico

V. Pérez-Reyes[a], R. M. Cabral-Lares[a,b], C. G. Méndez-García[c], R. Caraveo-Castro[a], I. A. Reyes-Cortés[d], J. Carrillo-Flores[a], and M. E Montero-Cabrera[a,*]

[a]*Centro de Investigación en Materiales Avanzados, Miguel de Cervantes 120, Complejo Industrial Chihuahua, 31109, Chihuahua, Chih. México.*
[*]*e-mail: elena.montero@cimav.edu.mx*
[b]*Tecnológico Nacional de México Campus Chihuahua II, Ave. De las Industrias #11101, Complejo Industrial Chihuahua, 31130, Chihuahua, Chih. México.*
[c]*CÁTEDRAS-CONACYT Instituto de Física de la UNAM, Circuito de la Investigación Científica, Ciudad Universitaria 04510, CDMX, México.*
[d]*Universidad Autonónoma de Chihuahua, Campus Universitario #2, Circuito Universitario, 31125, Chihuahua, Chih. México.*

Received 30 September 2021; accepted 23 May 2022

In Chihuahua, an important source of environmental radioactivity is found in the Sierra Peña Blanca, in the center of the state. The site comprises about 70% of uranium reserves in Mexico. The uranium of Peña Blanca was explored and partially exploited in the '80s. Due to the closure of operations, the extracted and unprocessed ore (hundreds of tons) was confined to rocky stacks, exposed to weathering. Subject to leaching, this uranium is transported from the mountains to Laguna del Cuervo. The mineral exposed in the repository and the uranium transport by surface water and recent sediments must be studied, to assess the effects on the environment, with radiometric and materials science techniques in conventional laboratories and synchrotron light. This work presents the study of sediment and pore water samples at various points along the lagoon, the values of the activity ratio of the 234U/238U isotopes and the sediment-water distribution coefficient of these isotopes, obtained by applying uranium liquid scintillation alpha spectrometry, gamma-ray spectrometry, scanning electron microscopy and X-ray diffraction methods.

Keywords: Peña Blanca; uranium; sediment; liquid scintillation.

DOI: https://doi.org/10.31349/SuplRevMexFis.3.010606

1. Introduction

The Sierra Peña Blanca is located 50 km north of the city of Chihuahua [1]. In the mountains range, there are uranium deposits associated with volcanic igneous rocks, the result of hydrothermal activity from high to low temperature, added to a high degree of volcanic activity, mainly felsic [2]. The rocks that host most of the uranium deposits in Peña Blanca are the Escuadra, Nopal and Coloradas formations. The principal deposits are Puerto III, Nopal I and Margaritas [3]. In the mentioned deposits, the primary uranium mineral (Uraninite) is scarce; secondary minerals are more frequent in high concentrations, such as the silicates alpha and beta-uranophane [Ca $(UO_2)_2(SiO_3)_2(OH)_2{\cdot}5H_2O$] and weeksite [$K_2$ $(UO_2)_2(Si_2O_5)_3{\cdot}4H_2O$], the vanadates carnotite [K_2 $(UO_2)_2(VO)_4{\cdot}3H_2O$] and tyuyamunite [Ca $(UO_2)_2(VO_4)_2{\cdot}5\text{-}8H_2O$], and the phosphate autunite [Ca $(UO_2)_2(PO_4)_2{\cdot}12H_2O$] [4]. The uranium of Peña Blanca was explored and partially exploited in the '80s. After the closure of operations, hundreds of tons of the extracted unprocessed ore were confined to rocky stacks as a repository, then exposed to weathering.

Laguna del Cuervo is located in the hydrological region RH34 "Cuencas Cerradas del Norte", Laguna del Cuervo sub-basin; physiographically it belongs to the "Sierras y Llanuras del Norte" province. The origin of the province is the folding of marine sequences (Mesozoic) formed on a Paleozoic and Precambrian basement. In addition, continental sediments and lava spills filled the tectonic basins, which generated the formation of endorheic basins such as Laguna del Cuervo. This area is characterized by a relief of alluvial plains and lacustrine plains surrounded by elongated volcanic mountains. The lacustrine plain is of the intermittent type, because it only contains water in rainy seasons, which are isolated, of short duration but of high intensity, with average annual rainfall of 312.8 mm. The prevailing climate is arid and extreme. Surface water has agricultural uses, especially as a watering hole for livestock, so organic waste is regularly present in the area [5].

Uranium can exist in five different oxidation states, of which only two species are stable. The U (IV) ion forms UO_2, hydroxide, hydrated fluorides, and phosphates of very low solubility, so it is common to find them in particulate matter, either suspended or precipitated and also adsorbed on mineral surfaces and organic matter. The U (VI) ion forms the uranyl ion $(UO_2)^{2+}$, UO_3 y U_3O_8 where the uranyl ion is soluble in water [6]. Most of the uranium minerals reported in Peña Blanca form uranyl ion compounds.

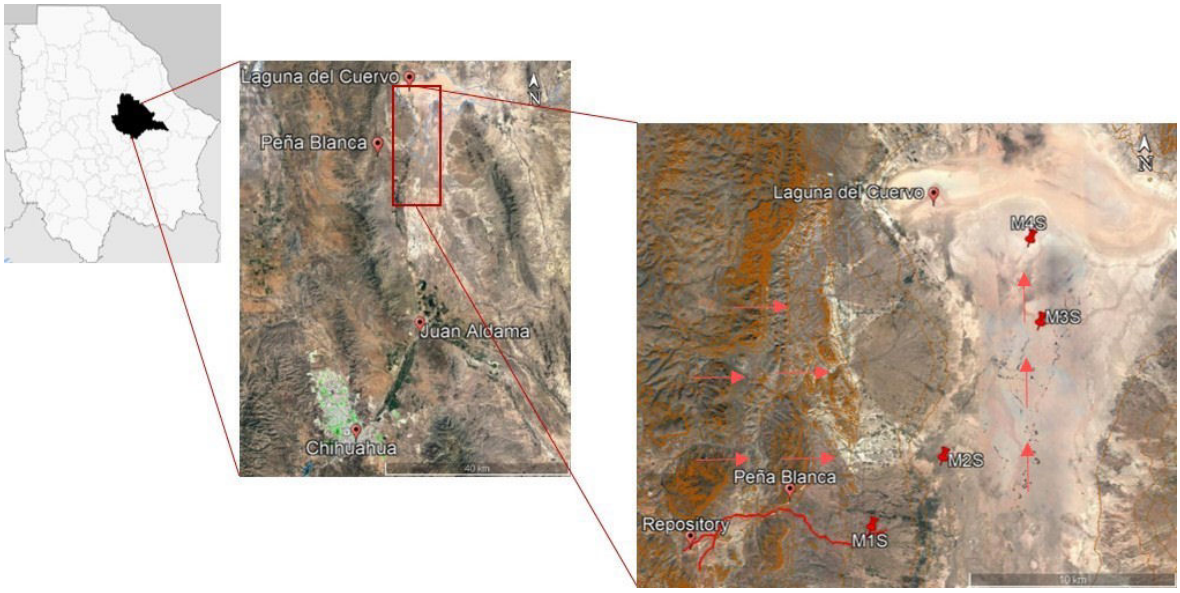

FIGURE 1. Satellite image of the study area. Distribution of the sample points, from 1 to 4 along the lacustrine plain of Laguna del Cuervo; the Boca Colorada stream is highlighted in red and the arrows indicate the flow of surface water from the repository to the deepest part of the lagoon.

The activity ratio (AR) is used as a geochemical tool to investigate the transport and flow relationships of uranium isotopes in waters [7]. If the activity concentrations Act (AU) of the corresponding isotopes are known, the activity ratio (AR) is defined as:

$$\mathrm{AR} = \frac{\mathrm{Act}(^{234}\mathrm{U})}{\mathrm{Act}(^{238}\mathrm{U})}. \tag{1}$$

How radioisotopes fractionate between water and sediments, both suspended and precipitated, is described by the distribution or partition coefficient (k_d), which expresses the concentration of radioisotopes adsorbed per unit mass of the solid, divided by the concentration of radioisotopes dissolved per unit volume of water [8].

$$k_d \left(\frac{\mathrm{m}^3}{\mathrm{kg}}\right) = \frac{\text{Isotope concentration in solid } \frac{\mathrm{Bq}}{\mathrm{kg}}}{\text{Isotope concentration in liquid } \frac{\mathrm{Bq}}{\mathrm{m}^3}}. \tag{2}$$

Radioisotopes, when decaying, may successively generate other radioisotopes, which are known as families or decay series. Radioisotopes ^{238}U and ^{235}U are the heads of the natural radioactive decay series, along with ^{232}Th. The health damage associated with uranium depends on its chemical and physical form, the route of incorporation, and the concentration of their radioactive isotopes. The uranium series radioactivity more dangerous to health by ingestion or inhalation is due to the short-lived alpha-active progeny isotopes, such as Ra, Rn, Po, and Bi, among others. The main concern of uranium is its direct chemical toxicity, as it is a heavy metal that obstructs the renal tissue [9].

In the present work the uranium-series isotope activities, activity ratios, and distribution coefficients from sediment and pore water samples at various points along the lagoon were determined, to clarify the distribution of uranium in the Laguna del Cuervo.

2. Materials and methods

The Sierra de Peña Blanca is located north of the city of Chihuahua at the coordinates 392758.94 m E, 3210556.22 m N (Fig. 1). Sample collection was performed at four points, which were selected on the path of the Boca Colorada stream following the natural flow of runoff water towards the deepest part of Laguna del Cuervo. This stream probably has the largest sedimentary contribution with uranium content, as it is the immediate drainage route from the uranium ore repository in the Sierra de Peña Blanca. The samples were deposited in previously washed plastic containers, which were filled with mud to the brim. At sampling points with surface water presence, a sample was taken separately in another container. All samples were preserved on ice from the collection during the transfer to the laboratory. There, the samples were refrigerated at 0 to 4°C for subsequent analysis. The parameters to be obtained are activity concentration Act ($^{\mathrm{A}}$U), AR, k_d.

Figure 2 shows the scheme of the characterization and measurement techniques used.

2.1. Scanning Electron Microscopy (SEM)

Morphological and elemental characterization was performed using a Jeol JSM 5800 LB equipment with the RX-S60/DX90 microanalysis energy-dispersive spectrograph (EDS). The acquisition of digital images was performed with secondary (SE) and backscattered (BSE) electrons.

2.2. X-ray diffraction (XRD)

The mineralogical analysis was performed by X-ray diffraction, using the XPERT-PRO PANalytical® equipment. The

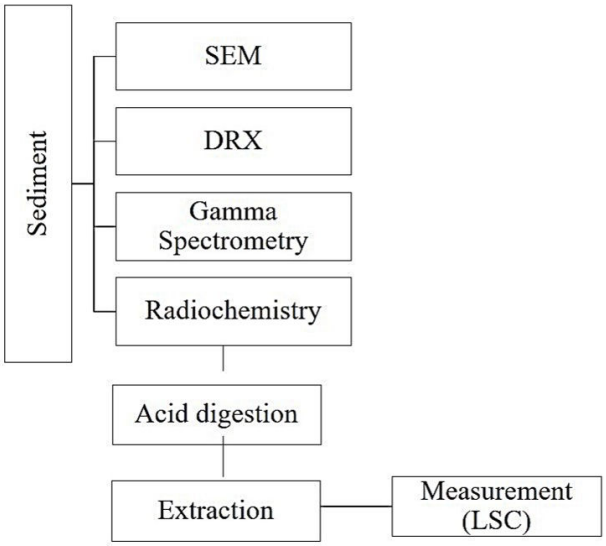

FIGURE 2. Methods used in the analysis of the samples.

analysis of the diffractogram was done using the Data Collector® software. CuKα radiation was used (current 40 mA and voltage 40 kV).

2.2.1. Rietveld method

The method quantifies the concentration of the crystalline phases of the sample, using a least-squares approach to refine a theoretical profile to fit a measured diffractogram [10].

2.3. Gamma spectrometry (GS)

For the GS measurement, a hyper pure germanium high-resolution gamma spectrometer Canberra model GC2020 with a relative efficiency of 20% was used. The determination of the activities was carried out by the relative method, using as standard the IAEA certified reference material RGU-1.

For the ^{238}U activity calculations, radioactive equilibrium of the ^{234}U or ^{226}Ra isotope is assumed. In closed geochemical systems, the cause of the radioactive disequilibrium between ^{226}Ra isotope and its daughters can be the ^{222}Rn gas escape from the sample container. Then, the dry sediment samples were deposited in hermetically sealed Teflon vials, to prevent the ^{222}Rn gas to escape. After 28 to 30 days the ^{222}Rn reaches equilibrium with the parent isotope ^{226}Ra.

The evaluation of the ^{226}Ra and ^{238}U equilibrium is essential due to their mobility differences. However, the energies of 186.21 keV of ^{226}Ra and 185.72 keV of ^{235}U lines are so close that reliable deconvolution cannot be done. If ^{226}Ra is guaranteed in equilibrium with its parent ^{238}U, and if the natural isotopic ratio ^{238}U/^{235}U is assumed, then from the appropriate nuclear data the number of counts corresponding to ^{226}Ra can be known. G. R. Gilmore [11] calculates the ratios of counts of the 186 keV peak area corresponding to ^{226}Ra and ^{235}U.

2.4. Uranium extraction and measurement

Uranium is presumed to be adsorbed or precipitated in sediments. To disintegrate the silicates and to avoid possible interferences in the liquid scintillator by organic materials, an acid digestion was carried out in an open system. Previously, the sample is taken to dryness for 24 h at 70°C and to calcined for 24 h to 600°C. The digestion was performed using, HF, Aqua regia and $HCLO_4$ [12]. Once free of color and sediment, the sample is evaporated to incipient dryness, subsequently, it is acidified with $HCLO_4$ and dried. The solid residue is dissolved with HNO_3 5M. The result is brought to total dryness.

Once the sample has been digested, the isotopes of interest are extracted. The sample is brought to medium sulfate, a necessary condition for the URAEX liquid scintillator-extractor to obtain the highest efficiency. The liquid scintillation alpha spectrometry measurement was made in the PERALS MODEL OP-312 spectrometer with an AIM-312 analyzer (ORDELA). The measurement time of each sample was 24 hours.

2.5. Liquid scintillation alpha spectrometry (LSC)

LSC is a versatile and sensitive technique for the detection and measurement of radioactivity [13]. Ionizing radiation interacts with the scintillating liquid, exciting and ionizing a large number of atoms and molecules, which when de-excited emit photons in the visible spectrum. The liquid scintillator is the first transducer, its photons are captured by a photomultiplier tube, whose signals are digitalized and further processed [14].

3. Results and discussions

The collection of samples was achieved in two periods, the first in June and the second in September 2018, at four sediment sampling points (Table I).

Samples M1S and M4S were analyzed by SEM. Figure 3 shows particles of different morphologies: spherical with diameters $\sim$ 10 μm, tabular with lengths $\sim$ 50 μm, clays $\sim$ 1 μm, as well as particles of irregular morphology. The variety of observed morphology and sizes suggests that the particles have been transported by saltation and/or rolling, and it is attributed to chaotic and intermittent behavior in the water flow. A semi-quantitative analysis was performed by EDS with BSE. Elemental analysis was used as a contribution to

TABLE I. Sampling points.

Sample	Coordinate		Matrix
M1S	404281 E,	3224208 N	Dry mud
M2S	407813 E,	3227513 N	Wet mud
M3S	412610 E,	3234022 N	Dry mud
M4S	412166 E,	3238054 N	Wet mud

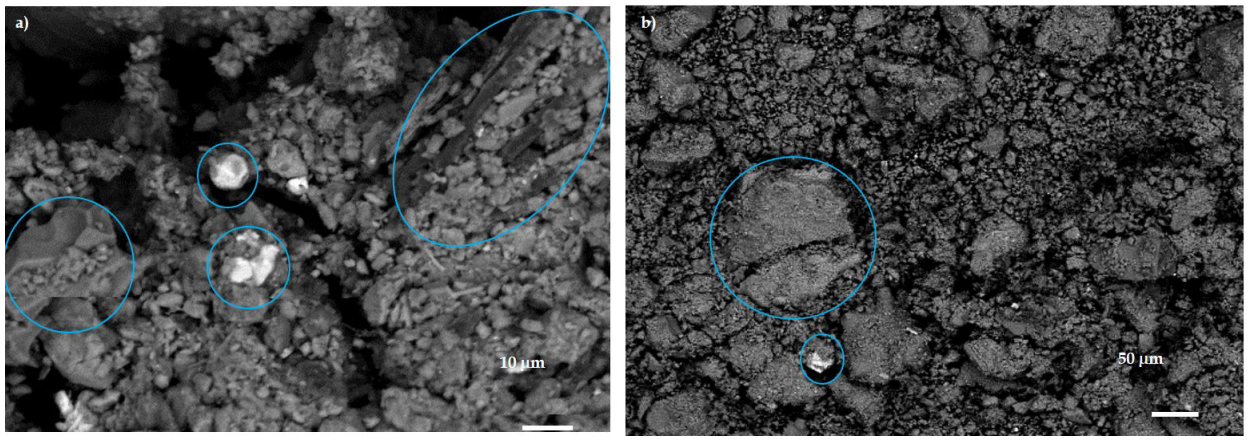

FIGURE 3. a) BSE image, magnification x1100. Sample M1S, grains of spherical shape $\phi \sim 10$ μm, tabular l$\sim$50 μm, and clays $\phi \sim 1$ μm, b) BSE image, magnification x200. Sample M4S.

TABLE II. Concentrations of mineral phases in sediments, obtained by the Rietveld method.

Sample	Mineral Phase (%)						
	Quartz	Calcite	Sanidine	Anorthite	Albite	Montmorillonite	Kaolinite
M1S	41.5 (0.8)	10.4 (0.4)	23.9 (0.9)	-	20.5 (0.3)	3.8 (0.2)	-
M2S	23.5 (0.7)	22.8 (0.4)	22.7 (0.9)	16 (1)	-	-	14.7 (0.2)
M3S	44 (1)	-	25.6 (0.7)	21 (1)	5.4 (0.4)	-	3.7 (0.8)
M4S	62 (2)	6.6 (0.2)	16.7 (0.8)	7.9 (0.5)	6.5 (0.4)	-	-

NOTE: Uncertainties are presented in parentheses (1σ).

identify the crystalline phases in the sediments. The diffractograms of the four samples were similar. The presence of quartz, calcite, feldspars (sanidine, anorthite, albite) and clays (montmorillonite and kaolinite), was observed. Since a wet separation of the clays was not carried out, the quantification was achieved by the Rietveld method analysis for the sediment samples, performed by the FullProf program (Table II) [10].

Radioactivity of samples was measured by GS as well as LSC. The ^{226}Ra activity was calculated according to the Gilmore method [11] through the intensity of the 186 keV doublet, in addition to being obtained by equating the activities of ^{214}Pb and ^{214}Bi, resulting from assuming radioactive equilibrium.

From this comparison, an estimate of the AR (^{234}U/^{238}U) can be made by GS. The results of these calculations are presented in Table III.

The samples M1S, M2S and M3S have an AR close to 1, while in M4S the AR is above 1. When the activity of ^{226}Ra obtained by the Gilmore relationship [11] is significantly lower than that obtained from the radioactive equilibrium, it can be deduced that the effective area calculated for the ^{235}U intensity is greater than the real one. Therefore, AR > 1 is feasible.

The activity determinations obtained by LSC are shown in Table IV. They cover a range from 37 ± 1 to 1740 ± 62 Bq/kg in ^{238}U and from 43 ± 2 to 1940 ± 69 Bq/kg in ^{234}U for the four samples. It can be observed that the $AR = 1.37$ obtained in the M4S sample has verified the results of GS discussed above. The sample M4S is in disequilibrium.

As observed in Table IV, the activity concentrations of ^{238}U and ^{234}U of the M2S sample in the sediment are up to 35 times higher than the rest of the results. Although Act (^{234}U) $>$ Act (^{238}U), the kd values have a higher sediment-pore water ratio for ^{238}U (kd: 4.7) than ^{234}U (kd: 4.3). This suggests a contribution of uranium from the water to the sediment by a reduction zone.

The high uranium concentration can be explained by a structural barrier present in the sampling area, approximately 1.5 km wide and a height that varies from 6 to 7 m. The barrier causes the stagnation of the retained runoff water, the presence of more plants and possible reducing agents.

TABLE III. Activity concentrations of ^{238}U isotope progenies and AR (^{234}U/^{238}U), determined by GS.

Sample	Radioisotope		AR	
	^{214}Pb (Bg/kg)	^{216}Bi (Bg/kg)	^{226}Ra (Bg/kg)	
M1S	72 ± 1	74 ± 2	69 ± 5	≈ 1
M2S	64 ± 1	67 ± 2	70 ± 5	≈ 1
M3S	77 ± 1	75 ± 2	79 ± 4	≈ 1
M4S	77 ± 2	76 ± 2	67 ± 5	> 1

TABLE IV. Comparison of results by sampling points.

Sample	Radioisotope	Sediments (Bq/kg)	AR	Pore water (Bq/m^3)	AR	k_d (m^3/kg)
M1S	^{288}U	50 ± 2	1.00 ± 0.05	-	-	-
	^{234}U	50 ± 2		-		-
M2S	^{238}U	1740 ± 62	1.11 ± 0.06	374 ± 14	1.2 ± 0.1	4.7
	^{234}U	1940 ± 69		447 ± 16		4.3
M3S	^{238}U	41 ± 1	1.03 ± 0.05	-	-	-
	^{234}U	43 ± 2	-	-		
M4S	^{238}U	37 ± 1	1.37 ± 0.06	332 ± 12	2.2 ± 0.1	0.1
	^{234}U	50 ± 2		719 ± 22		0.1

This area is used as a watering hole for local livestock, which produces organic waste that contributes to oxidation-reduction conditions.

The strong affinity that organic matter presents as a ligand for U has been studied by various authors (Chabaux, 2003 and authors cited there) [8]. During the early stages of deposition of organic debris, chemical-structural changes are produced by microbial decomposition [15,16]. One consequence of microbial activity is that, as oxygen is limited, reducing conditions are created in organic matter [15,17].

In this potential reduction zone, uranium can be precipitated or dissolved depending on the redox process it has undergone. For this reason, it is necessary to use molecular-scale methods of characterization in the different uranium compounds.

Currently, there are different techniques for the analysis of heavy metals and actinide elements, such as X-ray absorption fine structure spectroscopy (XAFS). This consistis of the modulation of the X-ray absorption coefficient at the absorption edges of the element. The regions of the spectrum are a) X-ray absorption near the edge structure (XANES); b) Extended X-ray absorption fine structure (EXAFS), from approximately 50 eV above the absorption edge. XANES is selective for chemical elements and allows the identification of uranium species and substrates. Synchrotron radiation is used to apply these methods [18].

A different option is X-ray photoelectron spectroscopy (XPS), in which the elemental composition, the empirical formula, and the electronic configuration of the elements found on the surface of the sample (10 nm) are measured, in which synchrotron light may or may not be used [19].

To perform the above mentioned methods, it is necessary to preserve the natural oxidation state of uranium in the sediment from its sampling. For this, the samples must be kept at low temperatures and in an anaerobic atmosphere with coating. In this way, the oxidation state is preserved for later analysis.

4. Conclusions

In this paper, the study area has an arid and extreme climate, with scarce but high-intensity rainfalls. When the great rainfall event occurs, it is when there is mobility of the uranium, dissolved or particulate, and the reduction conditions are produced. Therefore, uranium can be deposited in the area. Under these conditions the study was carried out. Thus, it is a typical case of uranium transport by surface waters from a natural uranium repository in an endorheic basin.

In sediments, the ^{238}U activity concentrations were from 37 ± 1 to 1740 ± 62 Bq/kg and in ^{234}U, from 43 ± 2 to 1940 ± 69 Bq/kg, producing AR from 1.00 to 1.37. The kd results of each radioisotope for different samples suggest that the runoff water carries particulate minerals from the repository towards the flooded lagoon together with dissolved uranium.

From Act (^{A}U), AR, k_d, and the local topography of the extraction point of the four samples, it is concluded that:

- The structural barrier probably creates a reduction zone.

- The runoff water avenues with dissolved uranium are accumulated in the study area. There, uranium is reduced at this structural barrier.

- The particulate mineral does not pass the barrier, the uranium in bulk remains in that area.

From the gamma spectrometry, it is corroborated that the oxidized water does not carry dissolved Ra and that the activity concentrations of the Ra correspond to the equilibrium of U and Ra in the bulk.

The species and the existence of different oxidation states of uranium in the bulk and its fractions should be identified, to relate them to their origin in the mineral deposit or repository, by applying X-ray absorption fine structure techniques at synchrotrons.

Acknowledgments

The authors acknowledge the CONACYT Frontiers Science 10853 project for supporting this research.

1. Consejo de Recursos Minerales, Monografía Geológico-Minera del Estado de Chihuahua, (Secretaria de Energía, Minas e Industria Paraestatal, Subsecretaría de Minas e Industria Básica, 1994) pp. 297. ISBN 9686710388, 9789686710380.
2. J. Villareal-Fuentes, G. Levresse, R. Corona-Esquivel, J. Tritlla, N. Piedad-Sánchez, Principales Anomalías de Uranio en México, AIMMGM (2011) 260. ISBN 978-607-95292-2-2.
3. P.C. Goodell, Geology of Peña Blanca uranium deposits, Chihuahua, Mexico, Uranium in volcanic and volcaniclastic rocks. *AAPG Stud. Geol*. *13* (1981) 275.
4. O. M. Munguía, Explicación genética y evaluación geoestadística del depósito de uranio Coneto-Buenavista, Mpio. de Rodeo, estado de Durango, Universidad Nacional Autónoma de México, (2005) 180.
5. Comisión Nacional del Agua, Actualización de la disponibilidad media anual de agua en el acuÃfero Laguna de Hormigas (0824), Estado de Chihuahua, (Comisión Nacional del Agua, 2015) pp. 1-7.
6. B. Bourdon, Introduction to U-series Geochemistry, Uranium Series Geochemistry: *Reviews in Mineralogy and Geochemistry (Mineralogical Society of America)*, **52** (2003) 1, https://doi.org/10.2113/0520001
7. A. Kumar *et al*., Activity ratios of 234U/238U and 226Ra/228Ra for transport mechanisms of elevated uranium in alluvial aquifers of groundwater in south-western (SW) Punjab, India, *Journal of Environmental Radioactivity* **151** (2016) 311, https://doi.org/10.1016/j.jenvrad.2015.10.020.
8. F. Chabaux, J. Riotte, O. Dequincey, U-Th-Ra Fractionation During Weathering and River Transport, Uranium Series Geochemistry: *Reviews in Mineralogy and Geochemistry (Mineralogical Society of America)* **52** (2003) 533, https://doi.org/10.2113/0520533.
9. UNSCEAR, Report to the General Assembly with Scientific Annexes (United Nations Publication, NY, 2000), pp 157-291. ISBN 92-1-142238-8.
10. J. Rodríguez-Carbajal, Recent advances in magnetic structure determination by neutron powder diffraction, *Physica B* **192** (1993) 55, https://doi.org/10.1016/0921-4526(93)90108-I
11. G. Gilmore, Practical Gamma-ray Spectrometry 2nd ed (Chichester: John Wiley & Sons, Ltd, Warrington, UK, 2008), pp. 319-322. ISBN 978-0-470-86196-7
12. I. Jarvis, K. Jarvis, Plasma spectrometry in the earth sciences: techniques, applications, and future trends, *Chemical Geology* **95** (1992) 1, https://doi.org/10.1016/0009-2541(92)90041-3
13. D. Skoog, J. Holler, S. Crouch, *Principios de análisis instrumental* 6ta ed, (Cengage Learning Editores, México, 2008), pp. 909-925. ISBN 0-495-01201-7.
14. N. Tsoulfanidis, S. Landsberger, Measurement & Detection of Radiation 4th ed (CRC Press, Boca Raton, 2015), pp. 195-216. ISBN 978-1-4822-1548-9.
15. S. Cumberland, G. Douglas, K. Grice, J. Moreau, Uranium mobility in organic matter-rich sediments: A review of geological and geochemical processes, *Earth-Science Reviews*, **159** (2016) 160, https://doi.org/10.1016/j.earscirev.2016.05.010.
16. B.D. Stewart *et al*., Influence of Uranyl Speciation and Iron Oxides on Uranium Biogeochemical Redox Reactions. *Geomicrobiology Journal* **28** (2011) 444 https://doi.org/10.1080/01490451.2010.507646.
17. J. Wan *et al*., Effects of Organic Carbon Supply Rates on Uranium Mobility in a Previously Bioreduced Contaminated Sediment. *Environmental Science & Technology* **42** (2008) 7573. https://doi.org/10.1021/es800951h.
18. M. Newville, Fundamentals of XAFS, *Reviews in Mineralogy & Geochemistry*, **78** (2014) 33 https://doi.org/10.2138/rmg.2014.78.2.
19. A. M. Beesley *et al*., *Evolution of chemical species during electrodeposition of uranium for alpha spectrometry by the Hallstadius method*, **67** (2009) 1559 https://doi.org/10.1016/j.apradiso.2009.03.031.